Available online at www.sciencedirect.com
ScienceDirect
Journal of Sound and Vibration 322 (2009) 987–1004
JOURNAL OF SOUND AND VIBRATION
www.elsevier.com/locate/jsvi

Dynamic analysis of bi-stable composite plates

Cezar G. Diaconu*, Paul M. Weaver, Andres F. Arrieta

Faculty of Engineering, University of Bristol, Bristol BS8 1TR, UK

Received 28 January 2008; received in revised form 15 November 2008; accepted 18 November 2008
Handling Editor: C.L. Morfey
Available online 8 January 2009

Abstract

The static and dynamic transitions between stable states for rectangular bi-stable laminated composite plates are considered. The laminated composite plates have nonsymmetric laminate configurations and are subjected to thermal curing in order to introduce residual stresses and to achieve bi-stability. As geometrically nonlinear effects occur, after curing, the plates are able to take multiple stable shapes at service or room temperature. A simple model for dynamic analysis of the snap-through phenomena is proposed based on strain field approximations for the plates. Hamilton's principle is applied in conjunction with the Rayleigh–Ritz method in order to achieve fast results. The model is used to evaluate the initial displacements for the stable states and also to investigate the static and dynamic transitions from one stable state to another. Parametric studies are carried out for various aspect ratios, laminate configurations and actuation loads and the results are compared with those obtained with finite element analysis in order to evaluate the accuracy of the model.

1. Introduction

Morphing structures are structures that change shape or state in order to change their operating characteristics or as a response to changes in the environmental conditions. Bi-stable or multi-stable structures are possible candidates for morphing structures because of their ability to remain in natural equilibrium after a shape change occurs. It is noted that some are currently used for deployable space structure applications [1–5]. Also, bi-stable plates have been proposed as high-lift device concepts for UAV or other aero-structures applications with morphing airfoils where the bi-stability of unsymmetric patches is used to drive the airfoil shape change [6,7].

Unsymmetrically laminated composite plates are promising morphing structures because they can take multiple cylindrical shapes when cooled from an elevated manufacturing temperature to the service or room temperature. Hyer [8] showed that multi-stability is a coupling phenomenon between the residual stresses induced by the thermal gradient due to cooling and the geometric nonlinearities given by the large out-of-plane deflections that appear within the structure. Later, Dano and Hyer [9] assumed polynomial approximations of the mid-plane strains of general unsymmetrically laminated bi-stable composite plates in order to predict their stable shapes using Rayleigh–Ritz minimization of the total potential energy. Cho et al.

*Corresponding author. Tel.: +44 117 33 17918; fax: +44 117 927 2771.
E-mail address: cz.diaconu@bristol.ac.uk (C.G. Diaconu).

0022-460X/$ - see front matter © 2008 Elsevier Ltd. All rights reserved.
doi:10.1016/j.jsv.2008.11.032

[10] provided numerical and experimental evidence that slippage between the tool plate and the laminate, during manufacturing, can reduce the curvatures of stable shapes by 25 percent. As these bi-stable composite plates can snap-through from one stable shape to another Dano and Hyer [11,12] extended their previous model to predict snap-through loads and developed an actuation solution based on shape memory alloys. Bi-stable composite plates actuated by piezoelectric patches were also studied by Schultz and Hyer [13] and by Portela et al. [14,15] who included environmental effects, specifically moisture absorption, in the analysis. Several studies [8,14,15] showed that, for plates with unsymmetric laminate configurations, bi-stability may be lost for hot and wet environmental conditions that lead to undesirable changes in the laminate shape and that bi-stability is enhanced for dry and cold conditions. Thus, these studies suggest that such bi-stable structures can be used in morphing airfoils applications, within the cooler range of typical flight conditions, these are temperatures from approximately -60 to $40\,^{\circ}\mathrm{C}$.

Although it is acknowledged that the snap-through is an almost instantaneous phenomenon [11,13], analytical studies on the snap-through dynamics were not found in literature. However, understanding the snap-through dynamics of bi-stable composites is important if such structures are to be used as morphing aerospace structures. This paper studies the dynamic transition between stable states for rectangular bi-stable laminated composite plates. The plates have nonsymmetric laminate configurations and are subjected to thermal curing in order to achieve bi-stability. As geometrically nonlinear effects occur, after curing, the plates are able to take multiple stable shapes at service or room temperature. The analytical model proposed by Dano and Hyer [11] is extended in this study in order to obtain fast results for dynamic analysis of bi-stable plates. Hamilton's principle is applied in conjunction with the Rayleigh–Ritz method in order to add inertial and damping terms to the model. The time dependency of the snap-through transition from one stable state to another and the role of the inertial and also damping terms are investigated. Parametric studies for initial deformations and for static and dynamic snap-through are carried out for various aspect ratios, laminate configurations and actuation loads. To investigate the accuracy of the model results are compared with those obtained from finite element modelling (FEM).

2. Problem formulation

This analytical model assumes that composite rectangular plates with general unsymmetric laminate configurations, were flat at manufacturing temperature and have been cooled to service or room temperature. The plates are fixed in the centre and have free edges. For dynamic analysis, the theory uses Hamilton's principle that states that the variation of Lagrangian function integrated with respect to time is zero [16]:

$$\delta \int_{t_0}^{t_1} L\,\mathrm{d}t = \delta \int_{t_0}^{t_1} (T + W_F - \Pi)\,\mathrm{d}t = 0, \tag{1}$$

where $L = T + W_F - \Pi$ is the Lagrangian function, T is the kinetic energy, W_F is the work of applied forces, and Π is the total potential energy.

2.1. Total potential energy

The total potential energy of the bi-stable plates contains the physical information that drives the bi-stability phenomenon as it includes the residual stresses induced by cooling and also the geometric nonlinearities given by the large out-of-plane deflections that appear within the plates [8]. The total potential energy Π in Eq. (1) is defined as:

$$\Pi = \int_{-L_x/2}^{L_x/2}\int_{-L_y/2}^{L_y/2}\int_{-H/2}^{H/2}\left(\frac{1}{2}\overline{Q}_{11}\varepsilon_x^2 + \overline{Q}_{12}\varepsilon_x\varepsilon_y + \overline{Q}_{16}\gamma_{xy}\varepsilon_x + \frac{1}{2}\overline{Q}_{22}\varepsilon_y^2 + \overline{Q}_{26}\gamma_{xy}\varepsilon_y + \frac{1}{2}\overline{Q}_{66}\gamma_{xy}^2 - (\overline{Q}_{11}\alpha_x + \overline{Q}_{12}\alpha_y + \overline{Q}_{16}\alpha_{xy})\varepsilon_x\Delta T - (\overline{Q}_{12}\alpha_x + \overline{Q}_{22}\alpha_y + \overline{Q}_{26}\alpha_{xy})\varepsilon_y\Delta T - (\overline{Q}_{16}\alpha_x + \overline{Q}_{26}\alpha_y + \overline{Q}_{66}\alpha_{xy})\gamma_{xy}\Delta T\right)dz\,dy\,dx, \tag{2}$$

where $\overline{Q}_{ij}$ are the transformed reduced stiffnesses of the individual layers, L_x, L_y are the length of the laminated plate in the x- and y-directions, H is its thickness, α_x, α_y, α_{xy} are the transformed coefficients of

thermal expansion and ΔT is the temperature change between the manufacturing temperature and the service or room temperature. The total strains ε_x, ε_y, ε_{xy} are given by

$$\varepsilon_x = \varepsilon_x^0 + z\kappa_x^0,$$

$$\varepsilon_y = \varepsilon_y^0 + z\kappa_y^0,$$

$$\gamma_{xy} = \gamma_{xy}^0 + z\kappa_{xy}^0, \tag{3}$$

with the mid-plane strains and curvatures defined to include von Karman geometrical nonlinearities:

$$\varepsilon_x^0 = \frac{\partial u^0}{\partial x} + \frac{1}{2}\left(\frac{\partial w^0}{\partial x}\right)^2,$$

$$\varepsilon_y^0 = \frac{\partial v^0}{\partial y} + \frac{1}{2}\left(\frac{\partial w^0}{\partial y}\right)^2,$$

$$\gamma_{xy}^0 = \frac{\partial u^0}{\partial y} + \frac{\partial v^0}{\partial x} + \frac{\partial w^0}{\partial x}\frac{\partial w^0}{\partial y}, \tag{4}$$

$$\kappa_x^0 = -\frac{\partial^2 w^0}{\partial x^2} = -a,$$

$$\kappa_y^0 = -\frac{\partial^2 w^0}{\partial y^2} = -b,$$

$$\kappa_{xy}^0 = -2\frac{\partial^2 w^0}{\partial x \partial y} = -c, \tag{5}$$

where u^0, v^0, w^0 are the mid-plane displacements of the laminate in the x, y, z-coordinate directions.

In order to use Rayleigh–Ritz method, the out-of-plane displacement is assumed as [9]

$$w^0(x,y) = \tfrac{1}{2}(ax^2 + by^2 + cxy), \tag{6}$$

where a, b, c are to-be-determined coefficients which represent, respectively, the negative of the curvatures in x- and y-directions and the negative of the twist curvature.

The extensorial mid-plane strains are approximated using the following set of complete polynomials:

$$\varepsilon_x^0 = d_1 + d_2x^2 + d_3y^2 + d_4xy,$$

$$\varepsilon_y^0 = d_5 + d_6x^2 + d_7y^2 + d_8xy, \tag{7}$$

where d_i are to-be-determined coefficients.

The in-plane displacements u and v can be determined by integrating the strain–displacement relations:

$$u_{,x}^0 = \varepsilon_x^0 - \frac{1}{2}\left(\frac{\partial w^0}{\partial x}\right)^2 = d_1 + d_2x^2 + d_3y^2 + d_4xy - \frac{1}{2}\left(ax + \frac{1}{2}cy\right)^2, \tag{8}$$

$$v_{,y}^0 = \varepsilon_y^0 - \frac{1}{2}\left(\frac{\partial w^0}{\partial y}\right)^2 = d_5 + d_6x^2 + d_7y^2 + d_8xy - \frac{1}{2}\left(by + \frac{1}{2}cx\right)^2. \tag{9}$$

By integrating Eqs. (8) and (9) with respect to x and y leads to, respectively,

$$u^0(x,y) = d_1x + \tfrac{1}{3}d_2x^3 + d_3xy^2 + \tfrac{1}{2}d_4x^2y - \tfrac{1}{6}a^2x^3 - \tfrac{1}{4}acx^2y - \tfrac{1}{8}c^2xy^2 + h(y), \tag{10}$$

$$v^0(x,y) = d_5y + d_6x^2y + \tfrac{1}{3}d_7y^3 + \tfrac{1}{2}d_8xy^2 - \tfrac{1}{6}b^2y^3 - \tfrac{1}{4}bcxy^2 - \tfrac{1}{8}c^2x^2y + g(x), \tag{11}$$

where $h(y)$ and $g(x)$ are the result of partial integration which are chosen of the following form:

$$h(y) = d_9 y + \tfrac{1}{3} d_{10} y^3,$$

$$g(x) = d_9 x + \tfrac{1}{3} d_{11} x^3. \tag{12}$$

In the above, the coefficient d_9 for x and for y is the same in order to eliminate the rigid body rotation in the $x-y$ plane from being part of the assumed displacements.

The in-plane displacements can be expressed as

$$u^0(x,y) = d_1 x + d_9 y + \tfrac{1}{2}(d_4 - \tfrac{1}{2}ac)x^2 y + (d_3 - \tfrac{1}{8}c^2)xy^2 + \tfrac{1}{3}(d_2 - \tfrac{1}{2}a^2)x^3 + \tfrac{1}{3}d_{10}y^3, \tag{13}$$

$$v^0(x,y) = d_9 x + d_5 y + (d_6 - \tfrac{1}{8}c^2)x^2 y + \tfrac{1}{2}(d_8 - \tfrac{1}{2}bc)xy^2 + \tfrac{1}{3}(d_7 - \tfrac{1}{2}b^2)y^3 + \tfrac{1}{3}d_{11}x^3. \tag{14}$$

The in-plane shear strain can be computed using the third strain–displacement relation:

$$\gamma^0_{xy} = 2d_9 + (ab - \tfrac{1}{4}c^2 + 2d_3 + 2d_6)xy + (\tfrac{1}{2}(\tfrac{1}{2}ac + d_4) + d_{11})x^2 + (\tfrac{1}{2}(\tfrac{1}{2}bc + d_8) + d_{10})y^2. \tag{15}$$

Note that the procedure outlined in this section, e.g. Eqs. (6)–(15), was previously derived by Dano and Hyer [9].

2.2. Work of applied forces

To be able to actuate bi-stable plates, that is, to snap the plates from one stable state to another, it is necessary to apply some actuation loads on the plates. Such loads can be applied using shape memory alloys [11,12], piezoelectric patches [13–15] or concentrated loads applied transversally on various locations on the plate. In the present study, for sake of simplicity, actuation loads are applied in the form of four concentrated transverse forces applied on the four corners of the plates at $x = \pm L_x/2$ and $y = \pm L_y/2$. In this case, the virtual work of applied forces in Eq. (1) becomes:

$$\delta W_F = 2f\left[\left(\frac{L_x}{2}\right)^2 \delta a + \left(\frac{L_y}{2}\right)^2 \delta b\right], \tag{16}$$

where f is the magnitude of the applied forces. Eq. (16) can also be written as a force function of a, b, c:

$$\mathbf{F}(a,b,c) = 2f\left\{\left(\frac{L_x}{2}\right)^2 \quad \left(\frac{L_y}{2}\right)^2 \quad 0\right\}^{\mathrm{T}}. \tag{17}$$

2.3. Total kinetic energy

For dynamic analysis studies, one should define the total kinetic energy in order to take into account the inertial forces that appear on a structure. The total kinetic energy T in Eq. (1) is defined for rectangular plates as

$$T = \frac{1}{2}\rho h \int_{-L_x/2}^{L_x/2}\int_{-L_y/2}^{L_x/2}\left\{\dot{u}^0 + \dot{v}^0 + \dot{w}^0 - \frac{h^2}{12}\left[\left(\frac{\partial \dot{w}^0}{\partial x}\right)^2 + \left(\frac{\partial \dot{w}^0}{\partial y}\right)^2\right]\right\} \mathrm{d}x\,\mathrm{d}y, \tag{18}$$

where $\dot{u}^0$ denotes $\dot{u}^0 = \partial u^0/\partial t$, etc. By integrating by parts so as to separate virtual displacements δu, δv, δw from differential operators, it can be shown that the time integration of the variation of total kinetic energy equates to the time integration of virtual work done by inertial forces:

$$\begin{aligned}\int_{t_0}^{t_1} \delta T\,\mathrm{d}t &= \int_{t_0}^{t_1} \delta W_u\,\mathrm{d}t \\ &= -\int_{t_0}^{t_1}\left\{\rho h \int_{-L_x/2}^{L_x/2}\int_{-L_y/2}^{L_y/2}\left\{\ddot{u}^0\delta u + \ddot{v}^0\delta v + \left[\ddot{w}^0 - \frac{h^2}{12}\left(\frac{\partial^2 \ddot{w}^0}{\partial x^2} + \frac{\partial^2 \ddot{w}^0}{\partial y^2}\right)\right]\delta w\right\}\mathrm{d}x\,\mathrm{d}y\right\}\mathrm{d}t,\end{aligned} \tag{19}$$

where δW_u is virtual work done by inertial forces and $\ddot{u}^0$ denotes $\ddot{u}^0 = \partial^2 u^0/\partial t^2$, etc. Since the plate is clamped in its centre, the in-plane inertial forces vanish and δW_u becomes:

$$\delta W_u = -\rho h \int_{-L_x/2}^{L_x/2} \int_{-L_y/2}^{L_y/2} \left[\ddot{w}^0 - \frac{h^2}{12} \left(\frac{\partial^2 \ddot{w}^0}{\partial x^2} + \frac{\partial^2 \ddot{w}^0}{\partial y^2} \right) \right] \delta w \, \mathrm{d}x \, \mathrm{d}y. \tag{20}$$

By substituting Eq. (6) into Eq. (20) and then integrating, the virtual work done by inertial forces is obtained in terms of curvatures a, b, c as

$$\delta W_u = -\frac{\rho h L_x L_y}{32} \left\{ \left[\frac{L_x^4}{10} \ddot{a} + \frac{L_x^2 L_y^2}{18} \ddot{b} - \frac{h^2 L_x^2}{9} (\ddot{a} + \ddot{b}) \right] \delta a + \left[\frac{L_x^2 L_y^2}{18} \ddot{a} + \frac{L_y^4}{10} \ddot{b} - \frac{h^2 L_y^2}{9} (\ddot{a} + \ddot{b}) \right] \delta b + \frac{L_x^2 L_y^2}{18} \delta c \right\}. \tag{21}$$

2.4. Equations of motion

It can be seen that Hamilton Principle in Eq. (1) states that time integration of total virtual work is zero:

$$\int_{t_0}^{t_1} \delta W_T \, \mathrm{d}t = \int_{t_0}^{t_1} (\delta W_u + \delta W_F - \delta \Pi) \, \mathrm{d}t = 0. \tag{22}$$

The assumed mid-plane curvatures and strains in Eqs. (5), (7) and (15) can be substituted into the total strains in Eq. (3). The initial displacements induced by thermal stresses and the snap-through loads can now be obtained from static analysis by ignoring the inertial terms of δW_u and equating to zero the first variation of the total virtual work in Eq. (22) with respect to the unknown coefficients a, b, c, d_i:

$$\delta W_T = \delta W_F - \delta \Pi = \frac{\partial W_T}{\partial a} \delta a + \frac{\partial W_T}{\partial b} \delta b + \frac{\partial W_T}{\partial c} \delta c + \sum_{i=1}^{11} \frac{\partial W_T}{\partial d_i} \delta d_i = f_a \delta a + f_b \delta b + f_c \delta c + \sum_{i=1}^{11} f_{d_i} \delta d_i = 0. \tag{23}$$

Since $\delta W_T = 0$ for every admissible virtual coefficient, a system of 14 algebraic equations can be obtained $f_{a,b,c,d} = 0$. Because f_d are linear functions with respect to d_i, these coefficients can be determined as functions of $\mathbf{x} = \{a,b,c\}^{\mathrm{T}}$, that is $d_i = d_i(\mathbf{x})$, $i = 1 \ldots 11$, and the system can be simplified to only three nonlinear equations:

$$\mathbf{K}(\mathbf{x}) - \mathbf{F}(\mathbf{x}) = \mathbf{0}, \tag{24}$$

where $\mathbf{F}(\mathbf{x})$ is the force function defined in Eq. (17) and $\mathbf{K}(\mathbf{x}) = \{\partial \Pi/\partial a, \partial \Pi/\partial b, \partial \Pi/\partial c\}^{\mathrm{T}}$ represents the nonlinear stiffness function. Two solutions for the initial displacements induced by thermal stresses can be obtained by setting the applied force to zero and solving the system in Eq. (24) using the Newton–Raphson technique. The snap-through load can also be obtained by gradually increasing the magnitude f of the applied forces until the system converges to only one solution. As some of the solutions may correspond to an unstable stress state, the stability of the solutions is identified by assessing if the Jacobian of $\mathbf{K}(\mathbf{x}) - \mathbf{F}(\mathbf{x})$ is positive definite or not. When one eigenvalue of the Jacobian is zero or negative, the matrix is not positive definite and the equilibrium solution is unstable.

The dynamic equations of motion can be obtained from Eq. (22) in the form:

$$\mathbf{M}\ddot{\mathbf{x}} + \mathbf{D}(\dot{\mathbf{x}}) + \mathbf{K}(\mathbf{x}) = \mathbf{F}(\mathbf{x}, t), \tag{25}$$

where $\mathbf{M}$ is the mass matrix which can be derived from Eq. (21):

$$\mathbf{M} = \frac{\rho h L_x L_y}{32} \begin{bmatrix} \frac{L_x^4}{10} - \frac{h^2 L_x^2}{9} & \frac{L_x^2 L_y^2}{18} - \frac{h^2 L_x^2}{9} & 0 \\ \frac{L_x^2 L_y^2}{18} - \frac{h^2 L_y^2}{9} & \frac{L_y^4}{10} - \frac{h^2 L_y^2}{9} & 0 \\ 0 & 0 & \frac{L_x^2 L_y^2}{18} \end{bmatrix} \tag{26}$$

and $\mathbf{F}(\mathbf{x},t)$ is the force function defined in Eq. (17) with the magnitude f depending on time, that is $f = f(t)$.

In order to take into account energy dissipation and to avoid constant snap-through between stable-states in the solution of the system equation, in Eq. (25), Rayleigh proportional damping is assumed:

$$\mathbf{D}(\dot{\mathbf{x}}) = \alpha \mathbf{M}\dot{\mathbf{x}} + \beta \mathbf{K}(\dot{\mathbf{x}}), \tag{27}$$

where α and β are the mass and stiffness damping coefficients. It will be shown later that the snap-through process occurs in the low frequency range, enabling us to consider $\beta = 0$ in Eq. (27) based on Kyriazoglou and Guild [17]. Thus, one only needs to determine from experiments a critical damping ratio ζ to which α is related by

$$\alpha = 4\pi\zeta\omega. \tag{28}$$

3. Analysis results

For benchmark studies, laminated composite plates are considered with width $L_x = 200\,\text{mm}$ and with aspect ratios $L_y/L_x = 1$ (square plates) and $L_y/L_x = 2$ (rectangular plates). The plates are subjected to thermal curing with a temperature difference of $\Delta T = -180\,^{\circ}\text{C}$ between the service and manufacturing temperatures in order to become bi-stable. The plates are made of graphite/epoxy material HexPly 8552 IM7 with the properties outlined in Table 1. The studies are carried out for cross-ply plates with 8, 12 and 16 layers and for plates with $[-45_4/45_4]_T$, $[30_4/60_4]_T$ and $[0_4/45_4]_T$ laminate configurations. The T subscript denotes that the laminate configurations are defined throughout the whole thickness of the plates.

In the following, the initial displacements after curing, the snap-through loads and the dynamic response of bi-stable laminated composite plates obtained with the analytical model are analysed and compared with results obtained by FEM (using ABAQUS [18]). The elements selected for analysis are S4R doubly curved shell elements with 4-nodes per element and reduced integration. The FEM meshes are chosen with a density of 20×20 elements for square plates and 20×40 for rectangular plates. These meshes were selected based upon several convergence studies in order to have a good compromise between precision and computing time of the analysis.

For studying initial stable states and snap-through loads, static FEM is carried out using five steps:

1. In the first step residual stresses are introduced by curing the bi-stable plate from an elevated temperature to service temperature. At the end of this step the plate takes one stable shape that is different from the initial manufacturing shape due to the induced residual stresses.
2. Actuation loads are applied to the plate in the second step in order to make it snap-through from one stable shape to another. During this step the magnitude of the snap-through load is determined for actuation from the first to second stable state as the load at which a sudden variation in the displacements is observed.
3. The loads are removed in the third step in order to ensure that the new shape of the plate is stable.
4. In the fourth step, the actuation loads are applied in the opposite direction in order to make the plate snap-through and return to the first stable shape. During this step the magnitude of the snap-through load is determined for actuation from the second to first stable state as the load at which a sudden variation in the displacements is observed.
5. During the fifth step, as done in the third step, the actuation loads are removed to ensure that the new shape is stable.

Table 1
Material properties for HexPly 8552 IM7.

Prop.	Fibre vol. [%]	Ply thick [mm]	Density [g/cm^3]	E_{11} [GPa]	E_{22} [GPa]	$G_{12} = G_{13}$ [GPa]	G_{23} [GPa]	ν_{12}	α_1 [°C]$^{-1}$	α_2 [°C]$^{-1}$
Value	57.7	0.131	1.57	164	12	4.6[a]	4.6[a]	0.3[a]	-1.8×10^{-8}[a]	3×10^{-5}[a]

[a]Stands for assumed.

During preliminary studies, two types of nonlinear static FEM, within ABAQUS, were evaluated: Riks analysis and static general analysis. Riks analysis has proven to be relatively unreliable because of its high dependence on the laminate configuration which required a cumbersome fine tuning for each step in order to reach stable results. On the other hand, static general analysis has proven to be robust and reliable for this problem when automatic stabilization with a damping factor of 10^{-7} was used during the analysis. Preliminary studies showed that both viscous forces and viscous damping energy generated by this damping factor were small when compared with overall forces and total strain energy, respectively. Thus, static general analysis, stabilized by a damping factor of 10^{-7}, is used for studying the initial stable states and the snap-through loads because of its robustness and reliability.

For studying the dynamic response of a bi-stable composite plate, the FEM is carried out using two steps:

1. The first step is a static general analysis in which residual stresses are introduced by curing the bi-stable plate from an elevated temperature to service temperature. At the end of this step, the plate takes one stable shape that is different from the initial manufacturing shape due to the induced residual stresses.
2. The second step is an implicit dynamic step in which time dependent loads are introduced together with mass and stiffness proportional damping coefficients. During this step, the dynamic response of the bi-stable composite plate is studied.

Note that, occasionally (e.g. for cross-ply square plates), at the end of first step, when the residual stresses are introduced, the plate may take an unstable saddle shape. This situation can be addressed by applying a small imperfection (e.g. loads or boundary conditions) on the plate during first step. Such small imperfection will ensure that the analysis will move away from the unstable shape and will converge to a stable shape. After the first step, this imperfection can be removed to ensure that the results are accurate.

3.1. Static analysis

The two initial stable states provide the initial displacements of the bi-stable plates after curing and are determined by solving the system in Eq. (24) and by nonlinear static FEM. Tables 2 and 3 show comparisons between results for analytical and FEM for the stable states initial displacements after curing. In these tables, w_1 and w_2 are transverse displacements at the corners and centre edges of the plates for first and second stable shape, respectively. For FEM analysis these values are the results obtained at the end of Step 1 for w_1 and, respectively, at the end of Step 3 for w_2. Several laminate configurations were considered. One can see that there are differences between the displacements w_1 and w_2 depending on aspect ratio, laminate configuration, and location on the plate.

In Table 2 the corner initial displacements of square cross-ply plate stable states exhibit discrepancies between the analytical results and FEM of 13% for $[0_4/90_4]_T$, 21% for $[0_6/90_6]_T$ and 23% for the $[0_8/90_8]_T$ laminate configurations. In the case of cross-ply rectangular plates, the discrepancies between analytical results and FEM for the corner initial displacements are approximately 7% for one stable state and between 20 and 70% for the second stable state. Such large discrepancies for the second stable state are given by the fact that, in this case, the initial displacements have small magnitudes and the boundary layer effect becomes important. This boundary layer effect is observed in the FEM results but does not appear in the analytical model because of constant curvature assumptions. A better match between analytical results and FEM is observed for the initial displacements at the centre of the plate edges rather than at the plate corners. In this case, the boundary layer effect is minimal for the centre edge that exhibits large initial displacements and maximal when the centre edge initial displacement is almost zero. In the following, only the results corresponding to minimal boundary layer effect will be analysed. In Table 2, the initial, centre edge displacements of square cross-ply plate exhibit discrepancies between the analytical results and FEM of 1 percent for $[0_4/90_4]_T$, 1.6 percent for $[0_6/90_6]_T$ and 5 percent for the $[0_8/90_8]_T$ laminate configurations. These results suggest that the analytical model behaves better for cross-ply square plates with high thickness ratio. However, for rectangular cross-ply plates with aspect ratio of two, the initial, centre edge displacements of first stable state exhibit discrepancies of 7.13 percent for $[0_4/90_4]_T$, 5.2 percent for $[0_6/90_6]_T$ and 2 percent for the $[0_8/90_8]_T$ laminate configurations. On the other hand, for these rectangular plates, the initial, centre edge displacements of second stable state exhibit discrepancies of

Table 2
Initial displacements for cross-ply plates with various thickness ratios—in (mm).

Aspect ratio	$L_y/L_x = 1$ (square plate)			$L_y/L_x = 2$ (rectangular plate)		
Laminate configurations	$[0_4/90_4]_T$	$[0_6/90_6]_T$	$[0_8/90_8]_T$	$[0_4/90_4]_T$	$[0_6/90_6]_T$	$[0_8/90_8]_T$
Analytical						
Displ. at $x = L_x/2,\ y = L_y/2$						
w_1	−21.07	−13.32	−8.34	−85.10	−56.12	−40.81
w_2	21.07	13.32	8.34	21.10	13.46	8.81
Displ. at $x = 0,\ y = L_y/2,\ x = L_x/2,\ y = 0$						
w_1	−21.20	−13.77	−9.50	−85.15	−56.27	−41.18
	0.13	0.45	1.16	0.05	0.153	0.37
w_2	−0.13	−0.45	−1.16	−0.18	−0.61	−1.48
	21.20	13.77	9.50	21.29	14.07	10.29
FEM						
Displ. at $x = L_x/2,\ y = L_y/2$						
w_1	−18.50	−11	−6.80	−79.51	−52.75	−37.80
w_2	18.50	11	6.80	17.35	9.65	5.14
Displ. at $x = 0,\ y = L_y/2,\ x = L_x/2,\ y = 0$						
w_1	−21	−14	−10	−79.48	−53.50	−40.40
	0.08	0.25	1.01	0.21	0.31	0.32
w_2	−0.08	−0.25	−1.01	−0.26	−0.15	−1.32
	21	14	10	22	14.83	10.77

Table 3
Initial displacements for plates with various laminate configurations—in (mm).

Aspect ratio	$L_y/L_x = 1$ (square plate)			$L_y/L_x = 2$ (rectangular plate)		
Laminate configurations	$[-45_4/45_4]_T$	$[-30_4/60_4]_T$	$[0_4/45_4]_T$	$[-45_4/45_4]_T$	$[-30_4/60_4]_T$	$[0_4/45_4]_T$
Analytical						
Displ. at $x = \frac{L_x}{2}, y = \pm\frac{L_y}{2}$						
w_1	−42.17	−39.37	−17.36	−95.35	−105.74	−57.93
	0.49	−2.42	−6.43	−10.03	−31.85	−36.25
w_2	−0.49	2.42	0.65	10.03	−0.15	−0.53
	42.17	39.37	23.13	95.35	73.74	44.61
Displ. at $x = 0,\ y = L_y/2,\ x = L_x/2,\ y = 0$						
w_1	−10.42	−15.78	−11.57	−42.15	−63.57	−46.70
	−10.42	−5.12	−0.33	−10.54	−5.23	−0.39
w_2	10.42	5.12	3.22	42.15	20.90	13.30
	10.42	15.78	8.68	10.54	15.83	8.74
FEM						
Displ. at $x = \frac{L_x}{2},\ y = \pm\frac{L_y}{2}$						
w_1	−43.95	−39.95	−18.60	−90.54	−101.65	−62
	3.18	−0.35	−3.11	−4.62	−28.15	−32
w_2	−3.18	0.35	1	4.84	−2.82	−2
	43.95	39.95	22.50	90.75	68.40	40
Displ. at $x = 0,\ y = L_y/2,\ x = L_x/2, \leftrightarrows y = 0$						
w_1	−10.38	−15.79	−11.50	−37.20	−59.82	−46
	−10.38	−4.93	−0.20	−12.02	−5.50	−0.43
w_2	10.38	4.93	2.95	37.75	18.80	12.25
	10.38	15.79	9	11.84	17.22	9.41

3.25 percent for $[0_4/90_4]_T$, 5.14 percent for $[0_6/90_6]_T$ and 4.4 percent for the $[0_8/90_8]_T$ laminate configurations. These results suggest that, in the case of rectangular cross-ply plates, the discrepancies between the analytical results and FEM do not depend on the thickness ratio of the plate.

In Table 3, the initial corner displacements of square plate exhibit discrepancies between the analytical results and FEM of 4 percent for $[-45_4/45_4]_T$, 1.5 percent for $[-30_4/60_4]_T$ and 4 percent for the $[0_4/45_4]_T$ laminate configurations. In the case of rectangular plates with aspect ratio of two, the discrepancies between the models for the first stable state are 5.3 percent for $[-45_4/45_4]_T$, 4 percent for $[-30_4/60_4]_T$ and 6.6 percent for $[0_4/45_4]_T$. For the second stable state, they are 5, 7.8 and 11.5 percent, respectively. Note, that in this case, the boundary layer effect is more difficult to assess as the displacement pattern is skewed for the reference x, y axes. Nevertheless, the discrepancies between the models for the initial, centre edge displacements of square plate are 0.4 percent for $[-45_4/45_4]_T$, 0.06 percent for $[-30_4/60_4]_T$ and 0.6 percent for $[0_4/45_4]_T$ for the first stable state. For the second stable state, the discrepancies between the models for the initial, centre edge displacements are 0.4 percent for $[-45_4/45_4]_T$, 3.8 percent for $[-30_4/60_4]_T$ and 3.6 percent for $[0_4/45_4]_T$. In the case of the first stable state for the rectangular plate with aspect ratio two, the discrepancies between the models for the initial, centre edge displacements at $x = L_x/2$ and $y = 0$ are 12.3 percent (13.3 percent) for $[-45_4/45_4]_T$, 5 percent (6.2 percent) for $[-30_4/60_4]_T$ and 8.2 percent (1.5 percent) for $[0_4/45_4]_T$. The percentage discrepancy given in parentheses corresponds to the initial, centre edge displacements located at $x = 0$ and $y = L_y/2$. Similarly, for the second stable state of the rectangular plate with aspect ratio of two, the discrepancies between the models for the initial, centre edge displacements are 11 percent (11.7 percent) for $[-45_4/45_4]_T$, 8.1 percent (11.2 percent) for $[-30_4/60_4]_T$ and 7.1 percent (8.5 percent) for $[0_4/45_4]_T$.

Overall, the comparison between results for analytical results and FEM, suggest that they are in relatively good agreement with best matched initial displacements observed at the centre edge of square plates with cross-ply $[0_4/90_4]_T$ and angle-ply $[-45_4/45_4]_T$ laminate configurations.

3.2. Static snap-through analysis

The static actuation loads at which the bi-stable plates snap-through from one stable state to another are determined, from Eq. (24), by increasing the magnitude f of the applied forces, in small increments, defined in Eq. (17). The system in Eq. (24) is solved for each increment until a single stable solution is obtained. In the FEM, nonlinear static analysis is employed to determine the snap-through (buckling) loads as explained in the introductory section of Section 3. Tables 4 and 5 show a comparison between the analytical model and FEM for snap-through loads. The results show that the analytical model over-predicts the FEM by 30–50 percent. The reason for these high differences is due to the fact that the analytical model restricts the plate to snap-through (buckle) following only cylindrically shaped displacement modes (or saddle shapes with constant curvature across the plate). Meanwhile, in the FEM, the plate can snap-through (buckle) following any possible displacement mode. For example, Fig. 1 shows the FEM shapes of (a) square and (b) rectangular cross-ply bi-stable plates with $[0_4/90_4]_T$ laminate configurations just prior to snap-through. One can see that the shapes predicted with FEM are not saddle shapes with constant curvatures across the plate as assumed in the analytical model. Such complex, noncylindrical snap-through modes were also observed experimentally by Potter et al. [19].

3.3. Dynamic snap-through analysis

Snap-through phenomenon from one stable shape to another is known to happen in a relatively short period of time. However, the snap-through process between two stable shapes is not an instantaneous process and dynamic analysis is necessary to fully characterize the phenomenon. In order to carry out the dynamic analysis, the dynamic equation of motion in Eq. (25) is transformed to

$$\begin{bmatrix} \mathbf{I} & \mathbf{0} \\ \mathbf{0} & \mathbf{M} \end{bmatrix} \begin{Bmatrix} \dot{\mathbf{x}} \\ \ddot{\mathbf{x}} \end{Bmatrix} = \begin{bmatrix} \mathbf{0} & \mathbf{I} \\ -\mathbf{K}(\,) & -\mathbf{D}(\,) \end{bmatrix} \begin{Bmatrix} \mathbf{x} \\ \dot{\mathbf{x}} \end{Bmatrix} + \begin{Bmatrix} \mathbf{0} \\ \mathbf{F}(\mathbf{x}, t) \end{Bmatrix} \tag{29}$$

and is time integrated using MATLAB function ODE15S—this function is based on a Runge–Kutta formula. In Eq. (29), $\mathbf{I}$ is the 3×3 identity matrix with values of one on the leading diagonal and zero elsewhere.

Table 4
Snap-through loads for cross-ply plates with various thickness ratios—in (N).

Aspect ratio	$L_y/L_x = 1$ (square plate)			$L_y/L_x = 2$ (rectangular plate)		
Laminate configurations	$[0_4/90_4]_T$	$[0_6/90_6]_T$	$[0_8/90_8]_T$	$[0_4/90_4]_T$	$[0_6/90_6]_T$	$[0_8/90_8]_T$
Analytical model	13.6	16.1	10.2	9.6 −25.6	15.3 −33.5	17.1 −31.1
FEM	9.3	11.8	8.1	5.6 −16.3	10.2 −21.3	14.6 −16.4

Table 5
Snap-through loads for plates with various laminate configurations—in [N].

Aspect ratio	$L_y/L_x = 1$ (square plate)			$L_y/L_x = 2$ (rectangular plate)		
Laminate configurations	$[-45_4/45_4]_T$	$[-30_4/60_4]_T$	$[0_4/45_4]_T$	$[-45_4/45_4]_T$	$[-30_4/60_4]_T$	$[0_4/45_4]_T$
Analytical model	11.1	11.7	3.3	11.9 −11.9	9.9 −15.7	2.3 −3.5
FEM	5.4	6	1.8	7.6 −7.6	7.6 −8	2 −2.3

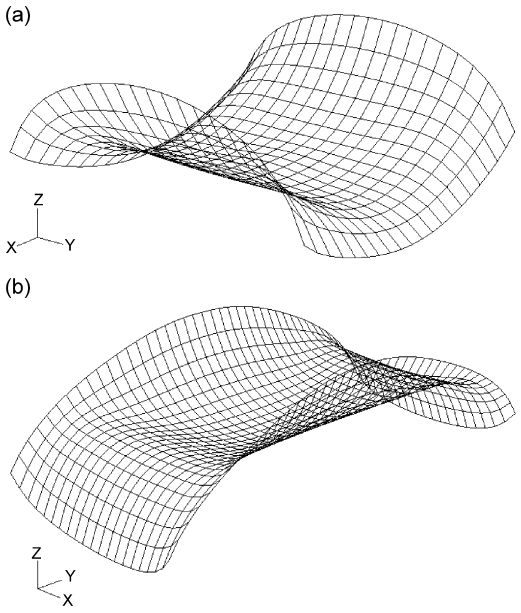

Fig. 1. Shapes of $[0_4/90_4]_T$ bi-stable plates prior to snap-through: (a) square and (b) rectangular.

The dynamic analysis is carried out for both an un-damped and a damped system of equations in order to investigate the role of inertial and energy dissipation (damping) terms. Because of large amount of data associated with dynamic analysis, in this study, attention is given only to cross-ply laminated composite plates due to their rather simple nature, e.g., zero twist curvature. Also, bi-stable cross-ply laminated composite plates are more likely to be used for practical applications compared with other laminate configurations as they are axially symmetric and, also, they tend to exhibit larger snap-through loads for similar thickness ratios.

3.3.1. Un-damped system

For the dynamic analysis on the un-damped system the energy dissipation terms $\mathbf{D}(\dot{\mathbf{x}})$ in Eq. (25) are ignored. Bi-stable square plates with $L_x = 200\,\text{mm}$ and $[0_4/90_4]_T$ laminate configuration clamped in their centre and subjected to transverse loads in their four corners are employed in order to investigate the role of the inertial terms in the analytical model. During analysis, the magnitude of the applied loads increases linearly for one second from zero to a given maximum value. After the first second, the applied loads are removed and the plates are allowed to oscillate freely.

The results are given in Figs. 2–5. The figures show the time dependencies of the: (a) displacements w of the plate corners, (b) curvatures a, b of the stable solution for which the loads are applied, and (c) loads magnitude f for several maximum magnitude values. Only the first four seconds of the analysis are shown in the figures. In the subfigures regarding the displacements w of the plate corners, the continuous line depicts the value of the first stable solution for which the loads are applied while the dot-dashed lines depicts the value of the second initial stable solution for the analytical model. In the subfigures regarding the curvatures, a and b are depicted with continuous and dashed lines, respectively.

Dynamic analysis was carried out for various maximum loads and suggests that the bi-stable plates snap to the second state for a maximum load magnitude of 15.5 N or above. Fig. 2 shows that for a given maximum load magnitude of only 10 N the plate does not snap. After the loads are removed, the plate oscillates around its original stable state with a frequency of 3.3 Hz.

For a maximum load magnitude of 15.5 N the results are given in Fig. 3. In this figure, it can be observed that the span-through is triggered by the accumulated kinetic energy (or inertial forces) because it occurs immediately after the actuation load was removed. It should be noted that for this analysis the snap-through duration is approximately 0.2 s. After snap-through, the plate oscillates with a frequency of 2.8 Hz around the second stable state following a nontrivial (nonsinusoidal) pattern due to the nonlinear nature of the system. It should also be noted that, during snap-through, the two curvatures are not simultaneously zero, that is, the plate is never flat but takes an intermediary saddle shape.

Due to the nonlinearity of the system, the time dependency pattern observed in Fig. 3 is highly dependent on the applied loads, that is, for very small increments, in the loads magnitude, completely different responses can be observed. In most cases, the plate snaps back to the first stable state and it oscillates between the two states. A stable time-dependency response can be identified for a range of maximum loads magnitudes between 23 and 24 N. This time-dependency response for displacements and curvatures is shown in Fig. 4 for a maximum load magnitude of 23.5 N. In this case, the snap-through occurs at approximately 0.7 s. After the curvatures

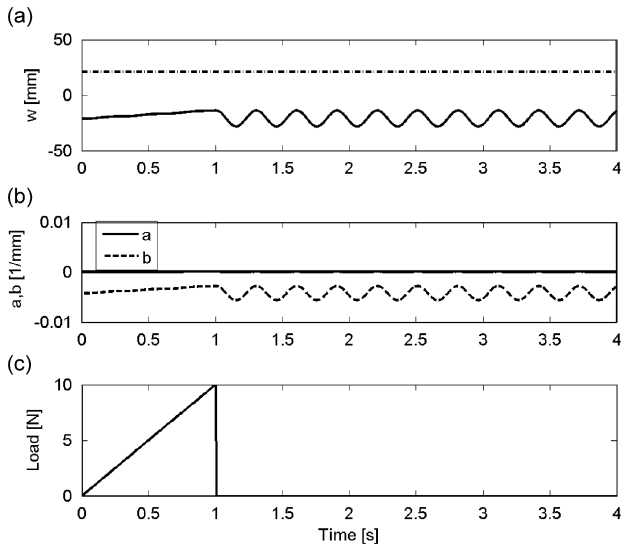

Fig. 2. Dynamic response for $[0_4/90_4]_T$ square plates subjected to a maximum load magnitude of 10 N. Time dependency of: (a) corner displacements w; (b) curvatures a, b; and (c) load magnitudes f.

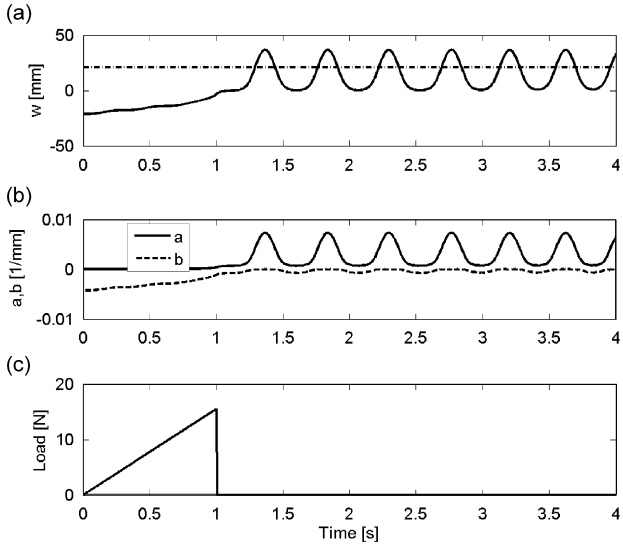

Fig. 3. Dynamic response for $[0_4/90_4]_T$ square plates subjected to a maximum load magnitude of 15.481 N. Time dependency of: (a) corner displacements w; (b) curvatures a, b; and (c) load magnitudes f.

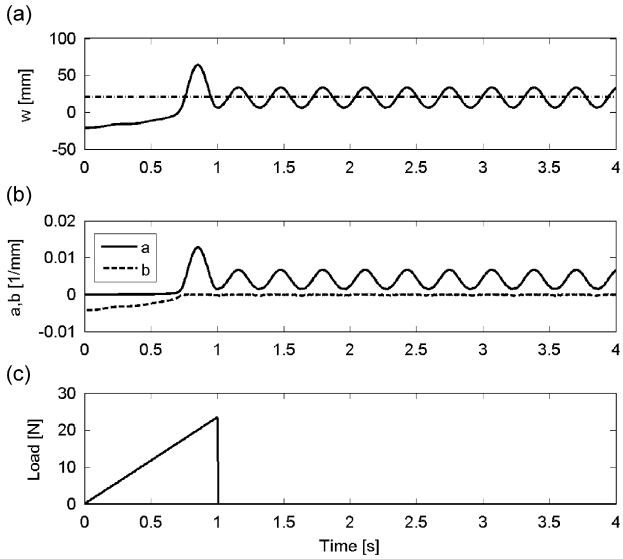

Fig. 4. Dynamic response for $[0_4/90_4]_T$ square plates subjected to a maximum load magnitude of 23.5 N. Time dependency of: (a) corner displacements w; (b) curvatures a, b; and (c) load magnitudes f.

and displacements reach a maximum at around 0.9 s, the plate tends to snap back due to the accumulated potential energy. However, the applied loads, which are still active, compensate this tendency and the plate remains oscillating with a frequency of 3.2 N around the second stable state. As previously observed, during the snap-through the plate is never flat but takes a saddle shape, that is, the curvatures a and b are never simultaneously zero.

For higher load magnitudes the behaviour of the plate is rather chaotic. Thus, in Fig. 5, the time-dependency response for displacements and curvatures is shown for a maximum load magnitude of 30 N. In this figure, it can be observed that the plate snaps through very quickly in both directions between the two stable states, following a highly nonlinear path. It should be noted that in this case the curves corresponding to the two curvatures intersect at zero, that is, the plate is flat, on many occasions.

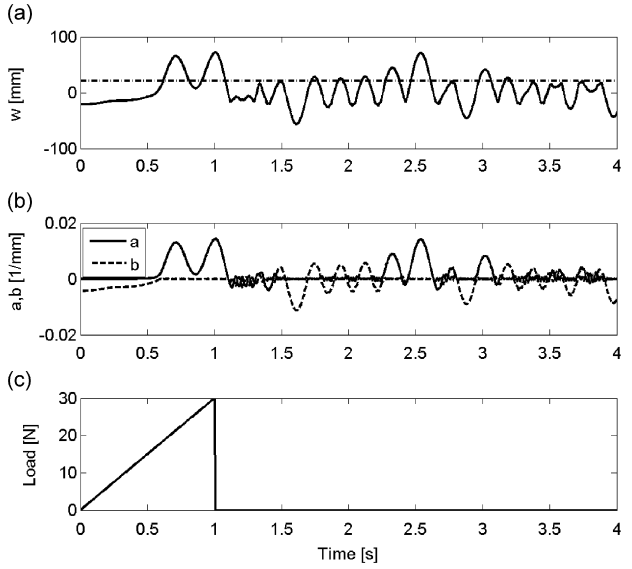

Fig. 5. Dynamic response for $[0_4/90_4]_T$ square plates subjected to a maximum load magnitude of 30 N. Time dependency of: (a) corner displacements w; (b) curvatures a, b; and (c) load magnitudes f.

The analysis on the un-damped system can offer valuable information about the role of the inertial terms on the behaviour of the bi-stable laminated composite plates. However, in experiments it was observed that the plates converge quickly to a stable state due to energy dissipation or damping.

3.3.2. Damped system

In order to carry out dynamic analysis on the damped system it is necessary to identify the dissipation terms $\mathbf{D}(\dot{\mathbf{x}})$ in Eq. (25). As stated in Eq. (27), Rayleigh proportional damping is assumed. As it will be shown in the following, the snap-through process occurs in the low frequency range, which allows one to consider $\beta = 0$ in Eq. (27). Thus, only the mass damping coefficient α should be experimentally determined in order to identify the dissipation terms $\mathbf{D}(\dot{\mathbf{x}})$. The mass damping coefficient α was determined from the free vibration response of a square plate with $L_x = 300$ mm and $[0_4/90_4]_T$ laminate configuration. The free vibration response was measured using a laser vibrometer. Fig. 6 shows the free response of the plate after being forced to oscillate at a frequency of approximately 30 Hz. This frequency was determined as the natural frequency at which large displacements appear on the plate corresponding to a snap-through mode. From these data, the critical damping ratio ζ was determined using the logarithmic decay method as $\zeta = 0.22$. The mass damping coefficient α was also calculated from Eq. (28) as $\alpha = 83$. Note that this benchmark study focuses on validating the analytical model against FEM rather than on matching experimental results. Therefore, the experimentally determined mass damping coefficient, $\alpha = 83$, is used in the dynamic analysis for different size plates than the one it is was determined for, even though, strictly, its value depends on plate dimensions.

The dynamic analysis is done for cross-ply plates with $L_x = 200$ mm and $[0_4/90_4]_T$ laminate configuration clamped in their centre and subjected to transverse loads in their four corners. The results are given in Fig. 7 for square plates and, in Fig. 8–11, for rectangular plates with aspect ratio $L_y/L_x = 2$. The figures show the time dependencies for (a) the vertical displacements w of a corner of the plate at $x = L_x/2$, $y = L_y/2$ and (b) the magnitudes of the applied loads. The analytical model is depicted by solid lines while the FEM is depicted by dashed lines. The dot-dashed lines depict the value of the second stable state for the analytical model. The analysis is carried out for sixty seconds in which the applied load is successively increased and decreased linearly with time.

In Fig. 7, the ratio between the loads applied in the analytical model and in the FEM dynamic analysis is the ratio between the snap-through loads identified in the previous section for the two models in Table 4. Thus, for the analytical model the maximum magnitude of the applied load is 15 N while for the FEM the maximum

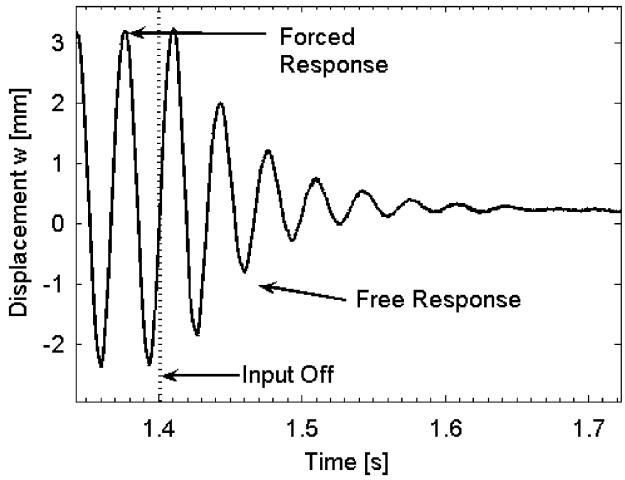

Fig. 6. Experimental free vibration response of a square plate with $L_x = 300\,\text{mm}$ and $[0_4/90_4]_T$ laminate configuration.

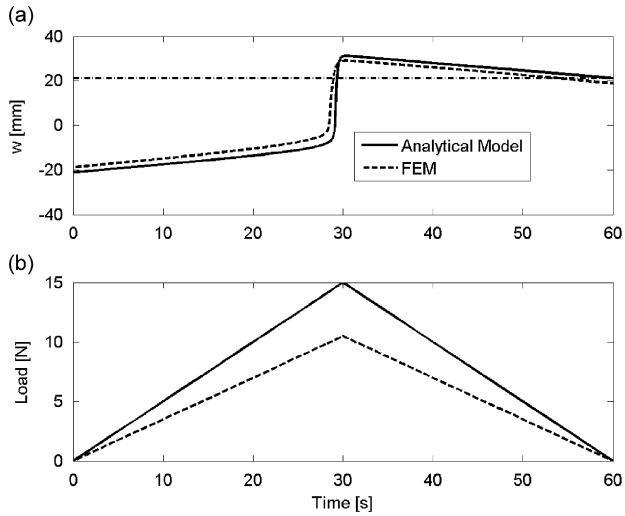

Fig. 7. Snap-through dynamics for a square plate with $[0_4/90_4]_T$ laminate configuration: (a) corner displacements w and (b) load magnitudes f.

magnitude of the applied load is 10.5 N. In Fig. 7, it can be seen that the time dependency for the vertical displacements for the two models are similar. The process of snap-through from the first stable shape to the second is observed to occur at approximately 29 s. However, the displacements from the FEM analysis have absolute values slightly smaller than the displacements from the analytical model as also observed when static analysis was carried out to identify the initial displacements.

Figs. 8 and 9 show the dynamics of the snap-through behaviour from first stable state to second stable state for rectangular cross-ply plates subjected to external loads. In Fig. 8, the maximum magnitude of the applied load is 15 N for the analytical model and 8.75 N for the FEM. The ratio between the two magnitudes equals the ratio between the magnitudes of the snap-through loads determined in Table 4. One can see that snap-through for the analytical model takes place after approximately 26 s. However, for the FEM the snap-through occurs after approximately 31 s. After snap-through, as the applied load is reduced, the displacements converge to the second stable solution, in both models. In Fig. 9, the maximum magnitude of the load is 15 N for both the analytical model and the FEM. While the behaviour of the displacements for the analytical model is identical with that in Fig. 8, in the FEM, due to the larger magnitude for the applied loads, the snap-through

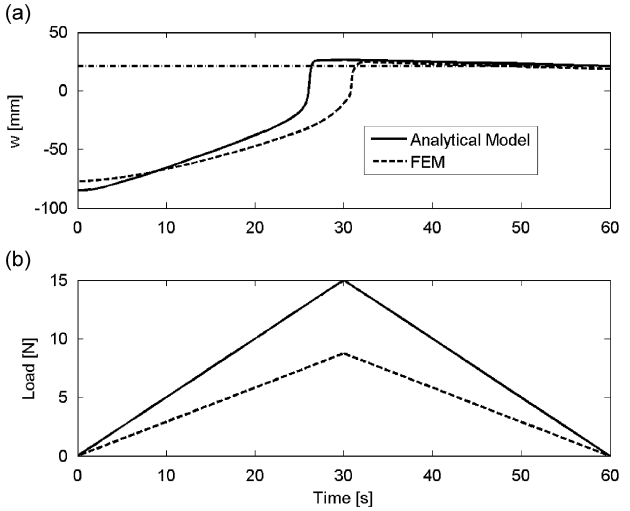

Fig. 8. Snap-through dynamics from first to second stable state for a rectangular plate with aspect ratio 2 and $[0_4/90_4]_T$ laminate configuration for models subjected to proportional snap-through loads: (a) corner displacements w and (b) load magnitudes f.

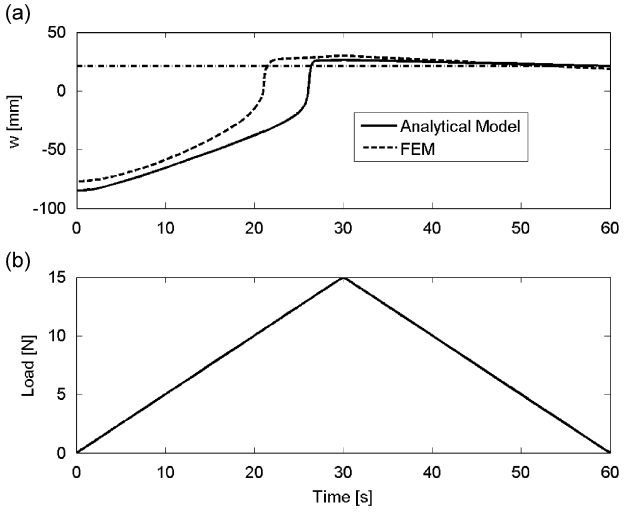

Fig. 9. Snap-through dynamics from first to second stable state for a rectangular plate with aspect ratio 2 and $[0_4/90_4]_T$ laminate configuration for models subjected to identical snap-through loads: (a) corner displacements w and (b) load magnitudes f.

occurs earlier at about 21 s. As in the previous case, after the snap-through, as the applied load is reduced, for both the models the displacements converge to the second stable solution. Note that, for both the proportional and same applied loads, after snap-through, the displacement paths followed by the two models are close to each other.

Figs. 10 and 11 show the dynamics of the snap-through behaviour from the second stable state to the first stable state for the same rectangular plates as in Fig. 8. In Fig. 10, the maximum magnitude of the applied load is 28 N for the analytical model and 17.9 N for the FEM. The ratio between the two magnitudes equals the ratio between the magnitudes of the snap-through loads determined in Table 4. In Fig. 10, it can be seen from the time dependency of the transverse displacements that the displacements for both the models intersect the second stable state at about the same time, which is around 31 s. For the FEM, the snap-through begins at approximately 28 s which is earlier than in the case of the analytical model. For the analytical model the snap-through begins at around 30 s. However, the snap-through phenomenon takes longer for the FEM compared

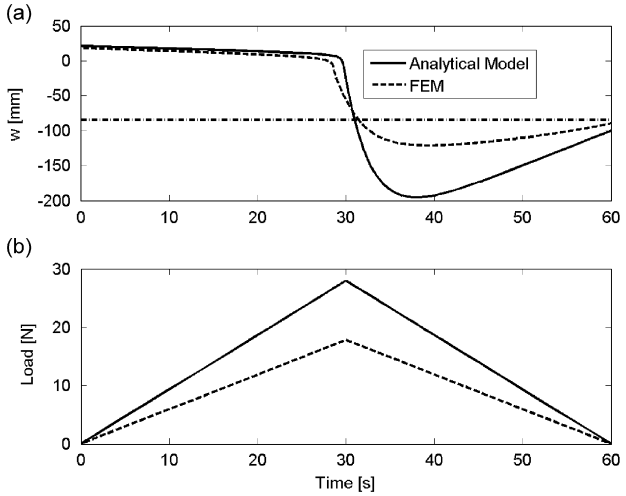

Fig. 10. Snap-through dynamics from second to first stable state for a rectangular plate with aspect ratio 2 and $[0_4/90_4]_T$ laminate configuration for models subjected to proportional snap-through loads: (a) corner displacements w and (b) load magnitudes f.

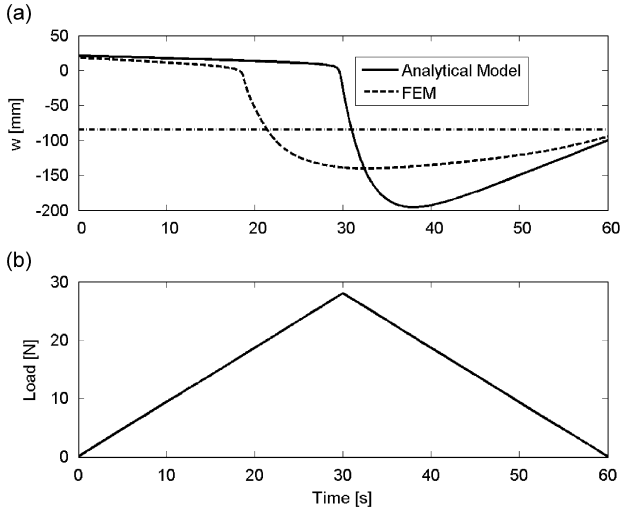

Fig. 11. Snap-through dynamics from second to first stable state for a rectangular plate with aspect ratio 2 and $[0_4/90_4]_T$ laminate configuration for models subjected to identical snap-through loads: (a) corner displacements w and (b) load magnitudes f.

with the analytical model. Also, after snap-through the amplitude of the transverse displacements is larger for the analytical model than for the FEM. For both models, after the snap-through, the displacements show similar behaviour. For example, the maximum displacement amplitudes, though different in magnitudes for the two models, occur at approximately 38 s. Also, as in the previous analyses, the displacements converge directly to the stable solution without oscillations. In Fig. 11, the maximum magnitude of the applied load is 28 N for both the analytical model and the FEM. In this case, the snap-through starts much earlier, for the FEM, at approximately 18 s. Also, after the snap-through, the maximum displacement appears at approximately 32 s for the FEM compared with 38 s for the analytical model. The magnitude of the maximum displacement amplitude is larger for the FEM in Fig. 11 compared with the magnitude of the maximum displacement amplitude for the FEM in Fig. 10. However, this magnitude remains lower than the maximum displacement amplitude for the analytical model.

When analysing Figs. 8–11, one can see that the differences between the analytical and FEM results are much larger when the plate snaps from the second to first stable shape. This discrepancy is due to the difference in the snap-through loads between the analytical model and FEM. Thus, as shown in Table 4, in the case of snap-through from the second to first stable shape, this difference is 9.3 N. This is larger than 4 N which is the difference between the models in case of snap-through from first to second stable shape. This fact makes the analytical model accumulate more potential energy prior to snap-through in the case of snapping from second to first state. When this energy is released during the snap-through from second to first stable shape, it makes the plate oscillate with a larger amplitude difference between the analytical model and FEM when compared with the snap-through in opposite direction.

4. Conclusions

For the static analysis the analytical model developed by Dano and Hyer [9] shows good agreement with the FEM. The most accurate results are observed for displacements at the centre of the plate edges rather than at the plate corners due to the boundary layer effect that appears on the FEM. This boundary layer effect cannot be predicted by this simple analytical model. However, the boundary layer effect is not significant for predicting the large deflections of bi-stable plates with free edges.

Regarding the snap-through analysis, the analytical model developed by Dano and Hyer [11], which is adopted in a simplified formulation in this study, over-predicts the magnitude of the snap-through loads by 30–50 percent compared with the FEM. These large differences are due to the fact that the analytical model restricts the plate to snap-through (buckle) following only cylindrical shape displacement modes (or saddle shapes with constant curvature across the plate). On the other hand, in the FEM, the plate can snap-through (buckle) following any possible displacement mode. Such noncylindrical modes were also observed experimentally by Potter et al. [19].

Using dynamic analysis the role of the inertial and damping terms on the snap-through between stable states of the bi-stable plates was identified. The results show that the analytical model developed in this study can be adjusted in some situations, e.g. cross-ply square plates or particular situations for cross-ply rectangular plates, to predict similar results to the FEM. Thus, it seems possible to calibrate the analytical model by adjusting the magnitude of the applied load and/or the damping parameters α, β in order to match not only the FEM, but also experimental results. Calibrating the analytical model in order to match experimental results will be the objective of further studies regarding the dynamic response of bi-stable composite plates.

References

[1] K.A. Seffen, Z. You, S. Pellegrino, Folding and deployment of curved tape springs, *International Journal of Mechanical Science* 42 (2000) 2055–2073.

[2] K.A. Seffen, Bi-stable concepts for reconfigurable structures, *Proceedings of the 45th AIAA/ASME/ASCE/AHS/ASC Structures, Structural Dynamics & Materials Conference*, Palm Springs, California, April 2004, AIAA Paper no. 2004-1526.

[3] T.W. Murphy, S. Pellegrino, A novel actuated composite tape-spring for deployable structures, *Proceedings of the 45th AIAA/ASME/ASCE/AHS/ASC Structures, Structural Dynamics & Materials Conference*, Palm Springs, California, April 2004, AIAA Paper no. 2004-1528.

[4] M.R.Schultz, M.J.Hulse, P.N.Keller, Neutrally stable composite tape springs, *Proceedings of the 47th AIAA/ASME/ASCE/AHS/ASC Structures, Structural Dynamics, and Materials Conference*, Newport, Rode Island, April 2006, AIAA Paper no. 2006-1810.

[5] P.N. Keller, M.S. Lake, D. Codell, R. Barrett, R. Taylor, M.R. Schultz, Development of elastic memory composite stiffeners for a flexible precision reflector, *Proceedings of the 47th AIAA/ASME/ASCE/AHS/ASC Structures, Structural Dynamics & Materials Conference*, Newport Rode Island, April 2006, AIAA Paper no. 2006-2179.

[6] F. Mattioni, P.M. Weaver, M.I. Friswell, K.D. Potter, Modeling and applications of thermally induced multistable composites with piecewise variation of lay-up in the planform, *Proceedings of the 48th AIAA/ASME/ASCE/AHS/ASC Structures, Structural Dynamics & Materials Conference*, Honolulu, Hawaii, April 2007, AIAA Paper no. 2007-2262.

[7] C.G. Diaconu, P.M. Weaver, F. Mattioni, Concepts for morphing airfoil sections using bi-stable laminated composite structures, *Thin Walled Structures* 46 (2008) 689–701.

[8] M.W. Hyer, Calculations of the room-temperature shapes of unsymmetric laminates, *Journal of Composite Materials* 15 (1981) 296–310.

[9] M.L. Dano, M.W. Hyer, Thermally-induced deformation behavior of unsymmetric laminates, *International Journal of Solids and Structures* 35 (1998) 2101–2120.

[10] M. Cho, M.H. Kim, H.S. Choi, H.C. Chung, K.J. Ahn, Y.S. Eom, A study of the room-temperature curvature shapes of unsymmetric laminates including edge effects, *Journal of Composite Materials* 32 (1998) 460–482.
[11] M.L. Dano, M.W. Hyer, Snap-through of unsymmetric fiber reinforced composite laminates, *International Journal of Solids and Structures* 39 (2002) 175–198.
[12] M.L. Dano, M.W. Hyer, SMA-induced snap-through of unsymmetric fiber-reinforced composite laminates, *International Journal of Solids and Structures* 40 (2003) 5949–5972.
[13] M.R. Schultz, M.W. Hyer, A morphing concept based on unsymmetric composite laminates and piezoceramic MFC actuators, *Proceedings of the 45th AIAA/ASME/ASCE/AHS/ASC Structures, Structural Dynamics & Materials Conference*, Palm Springs, California, April 2004, AIAA Paper no. 2004-1806.
[14] P.M. Portela, P.P. Camanho, P.M. Weaver, I.P. Bond, Analysis of morphing, multi-stable structures actuated by piezoelectric patches, in: C.A. Mota Soares, et al. (Eds.), *Proceedings of the Second ECCOMAS Thematic Conference on Smart Structures and Materials*, Lisbon, Portugal, July 2005.
[15] P.M. Portela, P.P. Camanho, P.M. Weaver, I.P. Bond, Analysis of morphing, multi-stable structures actuated by piezoelectric patches, *Computers and Structures* 86 (2008) 347–356.
[16] Y.Y. Yu, *Vibration of Elastic Plates: Linear and Nonlinear Dynamical Modeling of Sandwiches, Laminated Composites and Piezoelectric Layers*, Springer, New York, 1996, pp. 15–16.
[17] C. Kyriazoglou, F.J. Guild, Finite element prediction of damping of composite GFRP and CFRP laminates—a hybrid formulation–vibration damping experiments and Rayleigh damping, *Composites Science and Technology* 66 (2006) 487–498.
[18] ABAQUS, Finite Element Analysis, Software Package, Version 6.5, ABAQUS, Pawtucket, RI, URL: 〈http://www.abaqus.com〉, 2006.
[19] K.D. Potter, P.M. Weaver, A.A. Seman, S. Shah, Phenomena in the bifurcation of unsymmetric composite plates, *Composites Part A: Applied Science and Manufacturing* 38 (2007) 100–106.